Central Neurogenetic Signatures of the Visuo-Motor Integration System

Elisenda Bueichekú [a b] **Maite Aznárez-Sanado** [c d] **Ibai Diez** [a e] **Federico d'Oleire Uquillas** [f g] **Laura Ortiz-Terán** [a h] **Abid Y. Qureshi** [i j] **Maria Suñol** [a k l m] **Silvia Basaia** [a n] **Elena Ortiz-Terán** [a] **Maria A. Pastor** [c] **Jorge Sepulcre** [a i]

a: Gordon Center for Medical Imaging, Department of Radiology, Massachusetts General Hospital, Harvard Medical School, Boston, MA 02115;
b: Department of Basic Psychology, Clinical Psychology and Psychobiology, Jaume I University, 12071 Castelló de la Plana, Spain;
c: Neuroimaging Laboratory, School of Medicine, University of Navarra, 31008 Pamplona, Spain;
d: School of Education and Psychology, University of Navarra, 31008 Pamplona, Spain;
e: Neurotechnology Laboratory, Health Department, Tecnalia, E-48160 Derio, Spain;
f: Princeton Neuroscience Institute, Princeton University, Princeton, NJ, 08540
g: Department of Neurology, Massachusetts General Hospital, Harvard Medical School, Charlestown, MA 02129;
h: Department of Radiology, Brigham and Women's Hospital, Boston MA 02115;
i: Athinoula A. Martinos Center for Biomedical Imaging, Department of Radiology, Massachusetts General Hospital, Harvard Medical School, Charlestown, MA 02129;
j: Department of Neurology, University of Kansas Medical Center, Kansas City, MO 66160;
k: Psychiatry Department, Bellvitge University Hospital, Institut d'Investigació Biomèdica de Bellvitge - IDIBELL, 08907 L'Hospitalet de Llobregat, Barcelona, Spain;
l: Center for Biomedical Research in Mental Health Network, Carlos III Health Institute, 08907 L'Hospitalet de Llobregat, Barcelona, Spain;
m: Department of Clinical Sciences, School of Medicine, University of Barcelona, 08036 Barcelona, Spain;
n: Neuroimaging Research Unit, San Raffaele Scientific Institute, Vita-Salute San Raffaele University, 20132 Milan, Italy.

Corresponding Author: Jorge Sepulcre, sepulcre@nmr.mgh.harvard.edu

KEYWORDS: Visuo-Motor Integration, TBR1; Brain Functional Networks, Functional Connectivity, Genetics.

Acknowledgement: This research was supported by grants from the National Institutes of Health (NIH) (K23EB019023, R01AG061811, and R01AG061445 to J.S.). J.S. has no disclosures to report. E.B. was funded by a research stay grant from the Spanish Government (2017 *José Castillejo* for young Ph.D. researchers) and a postdoctoral research grant from the Generalitat Valenciana and the European Social Fund ("Investing in your future"; 2018 APOSTD).

Abstract

Visuo-motor impairments characterize numerous neurological disorders and neuro-genetic syndromes, such as Autism Spectrum Disorder (ASD), Dravet, Fragile-X, Prader-Willi, Turner and Williams syndrome. Despite recent advances in systems neuroscience, the biological basis underlying visuo-motor functional impairments associated with these clinical conditions is poorly understood. In this study, we used neuroimaging connectomic approaches to map the visuo-motor integration (VMI) system in the human brain, and investigated the topology approximation of the VMI network to the Allen Human Brain Atlas, a whole-brain transcriptome-wide atlas of cortical genetic expression. We found the genetic expression of 4 genes – TBR1, SCN1A, MAGEL2 and CACNB4 – to be prominently associated with visuo-motor integrators in the human cortex. TBR1 gene transcripts, an ASD gene whose expression is related to neural development of the cortex and the hippocampus, showed a central spatial allocation within the VMI system. Our findings delineate gene expression traits underlying the VMI system in the human cortex, where specific genes, such as TBR1, are likely to play a central role on its neuronal organization, as well as on specific phenotypes of neuro-genetic syndromes.

Significance

Previous research has explored the association between behavioral disorders and dysfunction in corresponding neural network. For example, Autism Spectrum Disorder, Prader-Willi syndrome and Dravet syndrome are characterized by behavioral deficits in the visuo-motor integration system. To date, few investigations have combined brain connectomic-genetic data to investigate the biological basis of childhood neurodevelopment and clinical syndromes. The present study provides evidence of a link between expression of malfunctioning genes associated with these syndromes (*i.e.*, TBR1, SCN1A, MAGEL2 and CACNB4) and cortical distribution across regions devoted to integrating visual and motor information (*i.e.*, the lateral occipital cortex, OP4 and intraparietal sulcus). We suggest this altered gene expression may underlie brain network dysfunction which, in turn, leads to behavioral deficits.

Introduction

Convergence of visual and motor neural circuits is fundamental for successful adaptation in humans. On a moment-to-moment basis, appropriate adjustment to a changing environment relies on a perception-action cycle, that is, the ability to process sensorial inputs and produce coherent motor responses. Not surprisingly, altered visuo-motor integration (VMI) has a profound functional impact on daily life motoric behaviors. A wide variety of neurological disorders and neuro-genetic syndromes have been associated with VMI dysfunction within the perception-action cycle. For example, syndromes such as Dravet (1-3), Fragile-X (4), Prader-Willi (5-7), Turner (8-10), Williams syndrome (11,12) and ASD (13,14) are characterized by compromised VMI in terms of the ability to interactively coordinate visual perception and fine motor skills (15-16). Though a great variety of genes have been proposed as a possible etiology for these syndromes (see SI Appendix, Table S1), some present phenotypic overlap and comorbidity between them (*e.g.*, Autism Spectrum Disorder and Fragile-X, Prader-Willi, Turner) (17-19). This under-appreciated pattern suggests the possibility that specific genetic backgrounds and interactions between genes could have direct effects on VMI-related circuits, in turn manifesting as atypical cognitive-behavioral adaptations to the changing environment.

To date, it remains unknown what genetic traits support the human VMI system. Following well-known clinical characterizations of the aforementioned neuro-genetic syndromes (ASD, Dravet, Fragile-X, Prader-Willi, Turner and Williams Syndrome), we hypothesized that the VMI network must overlap with specific patterns of gene expression along the brain's functional architecture, setting a substratum for typical and atypical VMI functioning. In this study, we aimed to first describe the cortical functional network that supports the visuo-motor integration system using a graph theory analysis based on functional connectivity MRI both at rest and task. Briefly, Cohort 1 participants completed a finger-tapping task during MRI scanning (see Methods and SI Appendix for more detailed information). The task consisted of learning and reproducing sequences of finger movements, thus integrating visual information and motor performance. Colored circles, which assigned a color to each finger, were used to present the sequence of finger movements (color 1: little finger, color 2: ring finger, color 3: middle finger, color 4: index finger). The only data used in our analysis was that which related to the ordered sequence of movements (*e.g.:* 1-2-3-

4-1-2-3-4) and the bimanual performance. Secondly, we used the Allen Human Brain Atlas (AHBA) (20) and genetic enrichment analyses (21) to examine genetic expression patterns delineated by the cortical map related to the visuo-motor integration system. Thirdly, we investigated the association between gene expression patterns of the VMI network and genes previously associated with neuro-genetic syndromes characterized by VMI impairments. In summary, we used a large-scale neuroimaging-connectomic-genetic strategy to unveil the brain connectivity supporting the VMI system and then uncovered the protein-coding genes whose gene expression profiles were most related to this system.

Results

Visuo-Motor Integration Maps. After performing a whole-brain voxel-level analysis of the VMI task, we found significant activation in lateral inferior and middle occipital cortex (BA 19, 37); sensorimotor cortex (BA 2, 3, 4 6); posterior middle temporal gyrus (BA 20, 21, 37), parietal opercula (OP1 to OP4), angular and supramarginal parietal cortices (BA 39, 40); supplementary motor area and dorsal anterior cingulate cortex (BA 24, 32), bilateral cerebellum (area 6, area 8, vermis 6, 7 and 8); and bilateral posterior fusiform gyri (BA 19) (Cohort 1, significance corrected threshold at q<0.001 False Discovery Rate (FDR); **Fig. 1A**).

Next, we calculated the brain areas that interconnect V1 and M1 using Stepwise Functional Connectivity (SFC), that is, areas that accumulate a high significant number of connections toward both, V1 and M1 concurrently (significance corrected threshold at q<0.001 FDR; **Fig. 1A**). This whole-brain voxel-level analysis was performed independently in task MRI data (Cohort 1) and resting-state MRI data (Cohort 2). We found that specific regions of the cerebral cortex display visuo-motor interconnector properties, namely, the medial and lateral inferior occipital gyri (BA 17, 18, 19); middle occipito-temporal cortex (BA 37); sensorimotor cortex (BA 2, 3, 4, 6); bilateral posterior fusiform gyrus (BA 19); precuneus and posterior cingulate gyrus; parietal opercula (OP1 to OP4), angular and supramarginal parietal cortices (BA 39, 40); supplementary motor area and dorsal anterior cingulate cortex (BA 24, 32); and anterior insula / inferior frontal cortex (BA 47, 48, 44, 45).

Finally, we obtained a consensus VMI map by averaging the normalized multimodal images, that is, the task activation, task connectivity and resting-state connectivity

maps, which highlighted the common brain areas involved in the performance of our VMI task and the interconnectivity between V1 and M1 (**Fig. 1B**). Medial occipital regions, specific areas of the motor cortex (BA 4 to BA 6), regions of the posterior to anterior cingulate gyrus including part of the precuneus, perisylvian areas (OP1 to OP4), and posterior to anterior insula and ventro-lateral inferior frontal gyrus were all found to be related to the integration of the visual and motor systems.

Genes with Cortical Expression within the Visuo-Motor Integration System. The VMI map displayed a high spatial similarity with 485 genes along the entire cerebral transcriptome of 20,737 genes from the AHBA. A Gene Ontology (GO) *Protein Analysis Through Evolutionary Relationships* (PANTHER) overrepresentation analysis of these 485 genes identified significant roles in specific *Biological Processes* and *Cellular Components* annotations (binomial test; significance corrected threshold at $q<0.05$ FDR; and fold enrichment (FE) >2). Particularly, we found that *cell communication by electrical coupling*, as well as different domains of the cellular *transmembrane transport* drove the main *Biological Processes* of the reported genes (**Fig. 1C**). This set of genes displayed an over-representation of specific *Cellular Components* circumscribed to *insulin receptor complex* (FE=26.75), *Na/P exchanging ATPase* (FE=14.86), *cation channel complex* (FE=2.97), as well as key parts of neurons such as *neuronal cell body membrane* (FE=8.26), *axon* (FE=2.03), and *GABA-ergic synapse* (FE=4.57). Moreover, we discovered that the cortical expression of four *a priori* genes selected from neuro-genetic syndromes with VMI alterations – *TBR1* ($r=0.606$; **Fig. 1D**), *SCN1A* ($r=0.526$), *MAGEL2* ($r=0.499$), *and CACNB4* ($r=0.489$) (see ***SI Appendix*, Fig. S1**) – had high spatial similarity with the VMI map (**Fig. 1C;** significance corrected threshold at $q<0.001$ FDR). An *interactome-based* validation approach with independent gene-gene interaction profiles demonstrated that TBR1, and to a lesser extent CACNB4 and MAGEL2, was centrally localized in its position within the genetic interaction network of the VMI-related genes (**Fig. 2A and B**). Results of another visualization approach are presented in see ***SI Appendix*, Fig. S2**. A visualization of the cortical distribution of the transcripts of TBR1, SCN1A, MAGEL2, and CACNB4 appears in ***SI Appendix*, Fig S3**.

Discussion

Successful performance of a variety of daily common tasks relies on the smooth interaction between visual processing and motor responses. Different neuro-clinical phenotypes and neuro-genetic syndromes have been related to behavioral deficits in the visuo-motor integration (VMI) system (*e.g.*, ASD: 22; Dravet Syndrome: 23, 3; Prader-Willi Syndrome: 6), or processes closely related to VMI, such as visual perception and fine motor coordination, or other cortical processes like motor inhibition and sustained attention (24). In this study, we aimed to close the gap in the understanding of the biological process behind perception-to-action in humans, and characterize the genetic basis underlying the integration of visual and motor functions. By doing so, we have delineated the cortical genetic background associated with VMI, where specific genes, such as *TBR1*, are likely to play a central role in its neuronal organization.

***Visuo-Motor Integration Network: Anatomical and Connectomic Theories*.** During the last few decades there has been a growing interest in studying and characterizing how the brain links perception-to-action (25). While segregation approaches, in which sensory and motor systems are studied in isolation, have been beneficial for understanding the numerous mechanisms that mediate functions of modal systems, there is a need for approaches that assess their direct integration in order to better understand brain system function, particularly in syndromes characterized by compromised goal-directed behavior. This is one of the main contributions of the present research: a connectomic approach was used to link brain activity during performance of a VMI task with brain anatomy and connectivity at rest. The finger-tapping task was used as an easy to implement task to study how brain processes visual information and produces coherent motor responses according to task goals. The brain network supporting the finger-tapping task highly overlapped with resting-state functional connectivity of the primary visual cortex and the primary motor area. A final consensus map allowed us to describe a fine-tuned map of the VMI regions in the human brain. This emphasized the role of the lateral occipital, intra-parietal sulcus (IPS) and perisylvian regions in the OP and frontal operculum areas as the main regions supporting the topology of the VMI network. Activity in the lateral occipital cortex has been associated with specific object representations in the visual cortex (26). This area responds to both visual and haptic object recognition, and the response is greater when the object is presented in these modalities at the same time (27-29). OP4 has been identified as a key region for sensorimotor integration (30, 31). Its activity has been associated with hand visuo-motor

stimulation (32, 33), finger object manipulation, discrimination and recognition (34, 35), as well as motor learning and visual perceptual-related functions after motor learning (36, 37). The intraparietal sulcus is a well-described attention area that supports the integration of visual inputs and cognitive information by using *priority maps* (e.g., 38-43). At the functional level, the intraparietal sulcus has been related to visuomotor integration in studies involving static (44) and moving objects (45).

Neuroimaging evidence found in the present research is well aligned with cognitive theories related with visual processing, motor programming, and the integration of visual and motor information, for example, the dorsal and ventral pathways of information processing (46) or the mirror neuron system (47). In accordance with results from the current study, previous research has found strong connectivity between parietal and premotor areas (48-50); also, a multimodal integration network comprising frontal, parietal and temporo-parietal areas has been described (51, 52). Accordingly, we found that brain areas were visual and motor information converge – the lateral occipital, the IPS and perisylvian regions in the OP and frontal operculum – delineate the VMI network.

Neuroimaging-Genetics of the Visuo-Motor Integration System. The combination of neuroimaging and genetic information is a promising tool for discovering key biological features of the VMI brain system. Using our consensus map and the AHBA, we were able to identify a set of genes whose cortical expression had highly significant spatial similarity to the VMI network. We observed that this VMI-spatially-related gene set exhibited cellular overrepresented functionalities in key domains for cellular and neuronal communicability (e.g. membrane transport, axons of neurons, or GABAergic synapses). Importantly, among all the genes detected, we found that the cortical expression of four genes from our pre-selected group of neuro-genetic syndromes – TBR1 [ASD (53, 54)], MAGEL2 [Prader-Willi Syndrome (53, 54)], SCN1A and CACNB4 [Dravet Syndrome (3, 55-59)] – displayed a high spatial overlap with the VMI map. While the exact implications of these four genes in VMI remain speculative, all of them are known to support molecular functions crucial for optimal development and communication between neurons. For instance, TBR1 expression has been related to the control of neural development in different brain regions (60-61). Previous studies have uncovered the genetic link between TBR1 and increased risk for ASD (53, 62). At the behavioral level, several studies have found VMI deficits (22, 63, 64) and motor

impairment in individuals presenting with ASD (65, 66). It is likely that the high expression of TBR1 in the VMI network may result in neuronal changes impacting its functionality, conferring prototypic behavioral phenotypes in ASD individuals. Moreover, almost one fifth of patients with Prader-Willi Syndrome also present ASD symptoms, and MAGEL2 mutations could be the cause of this comorbidity (54, 67, 68) MAGEL2, which is predominantly expressed in the brain, has been associated with neuronal differentiation and neuronal maintenance (69, 70). Similar to ASD, individuals with Prader-Willi Syndrome present VMI difficulties, including impairments in visual perception and motor coordination (5-7, 24, 71-72). In these patients, VMI abilities decline with age (5,6). Finally, some associations could be made between the alteration of voltage-gated sodium channels - which can lead to nervous system disorders, such as Dravet syndrome - and SCN1A mutations that cause functional impairments in the inter-communicability of brain neurons through GABAergic connectivity (59, 73-78). Moreover, CACNB4 mutations –also related to Dravet syndrome - are biologically related to calcium channels, which control synaptic transmission at neuronal terminals (55, 58). The combination of SCN1A and CACNB4 mutations may result in particularly aggravated clinical conditions associated with Dravet syndrome (55, 79). During the early stages of Dravet syndrome, there is often a disruption of neuronal communicability, which produces early visual and visuo-motor dysfunctionality (3). Overall, our findings provide insights about the potential neurobiological bases for common VMI impairments in specific neuro-genetic syndromes. We report 485 genes associated with VMI; candidate genes requiring further exploration to investigate potential novel genotypes associated with these and other VMI-related disorders. Future studies with larger sample sizes and/or specific clinical cohorts featuring some of the syndromes studied here (i.e. ASD, Prader-Willi Syndrome or Dravet Syndrome) would be ideal in this regard. The methodological approach used here could also be used for studying other phenotypic features in these and other central nervous system syndromes. Further investigation may help close the gap between observed symptoms and biological underpinnings. In future years, high-resolution brain transcriptomic data, like the AHBA, will likely become more widely available. This increased availability would improve our ability to understand how the brain functions across multiple scales, particularly in the interaction between genetic expression and functional network processing.

Conclusions. Our characterization of multimodal interactions (visual and motor cortices) in a specific VMI network facilitates the study of perception-to-action processes and allows the investigation of its underlying neurobiology. We first studied the neuroimaging-genetic relationships across the cortical mantle, following the framework that VMI is shaped by topological overlap between brain activity (goal-directed and spontaneous), connectivity, and genetic interactions. Although additional experimental work is needed to fully understand the relationship between genes of the VMI network system and behavioral impairment, we have described key intersections between the VMI and cortical genes with the help of the AHBA and clinical-genetic knowledge of several neuro-genetic syndromes. We showed that our findings regarding TBR1 (ASD), and to a lesser extent MAGEL2 (Prader-Willi), SCN1A (Dravet) and CACNB4 (Dravet), are not only relevant protein-coding genes within the neuronal systems of VMI, but are also likely important in the understanding of VMI impairments and neurocognitive development of the VMI cortical system.

Methods

Participants. We used data from two different cohorts. Cohort 1 consisted of 23 participants (8/15 female/male; mean age=56.39 years old, standard deviation, SD=8.60; range=42-74) that completed a Magnetic Resonance Imaging (MRI) experiment comprising of a high-resolution anatomical scan and a task-activation scan. All participants included in the sample were right-handed (80) and had normal or corrected-to-normal vision. Additionally, all participants were screened for neurological or psychiatric history and reported no past or current drug use. Participants provided written informed consent and all research protocols were approved by the University of Navarra Research Ethics Committee. Cohort 2 consisted of 23 participants (8/15 F/M; mean age=56.70 years old, SD=9.00; range=41-75) from The Brain Genomics Superstruct Project database (http://neuroinformatics.harvard.edu/gsp). Participants in cohort 2 were selected according to their handedness (right-handed), age and sex according to match characteristics of Cohort 1. Participants in Cohort 2 completed a full MRI and neuropsychological protocol [details available on (81)]. Only the high-resolution anatomical scan and the resting-state scan were used in the present study.

Functional MRI Task, Data Acquisition and Image Pre-processing. Visuo-motor integration task, data acquisition and image pre-processing details are provided in Supporting Information.

Image Post-processing

Task Activation Analysis. The task activation effects in each voxel were estimated by the General Linear Model and by modeling the data at the block level (SPM12 Wellcome Department of Imaging Neuroscience, London, England; www.fil.ion.ucl.ac.uk/spm/). The blood oxygenation level-dependent (BOLD) signal was estimated through the convolution of the stimuli with the canonical hemodynamic response function (HRF). Six motion realignment parameters were included to explain signal variations due to head motion, that is, as covariates of no interest. From the ordered sequence of movements, the first-level analyses resulted in two contrast images: 1) visual condition and 2) execution condition. In second-level analyses a mean image of the tapping task was obtained after conducting a whole-brain one-sample *t*-test analysis. The results were $q<0.05$ FDR voxel-level corrected. The corrected task-activation map was normalized using a *z*-score normalization approach.

Stepwise Functional Connectivity Analysis. The Stepwise Functional Connectivity (SFC) analysis has been described as a network analysis technique to investigate the integration of information from different brain systems at the functional connectivity level (52). In the present study, SFC analysis was used to describe a functional connectivity pathway that supports the integration of perception-action processes, more specifically the integration of visual and motor connectivity. In-house developed coding was used for SFC analysis that was run in Matlab software (Matlab R2015b, Natick, Massachusetts: The MathWorks Inc.). Briefly, a mask of 6,185 voxels covering the entire brain was used and SFC analyses were conducted at the individual level: *(i)* obtain connectivity matrices by calculating Pearson product-moment correlation coefficients (*r-values* and their *p-values*) for the time course of all brain voxels in a pairwise manner, obtaining the *r-value* matrix and the *p-value* matrix for each participant and each set of images; *(ii)* retain positive correlations to eliminate deleterious associations between voxels due to interpretational ambiguity (82, 83); *(iii)* correct each individual's connectivity matrix by controlling for the rate of false positives with a FDR approach [(84); a $q<0.001$ FDR correction was applied to the *p-values* matrix, resulting in only *r-values* with corrected *p-values*)]. These final individual association matrices (*i.e.*, corrected *p-value* matrices as weighted graphs) were used for the SFC analysis (represented as a simplified brain graph in **Fig. 3B**). For the subsequent SFC analysis, seed regions located in the primary visual cortex (left V1: MNI -6 -77 11; right V1: MNI 10 -77 9) and primary motor cortex (left M1: MNI: -30 -13 65 and right M1: MNI 34 -13 65) were defined as 3 mm radius spheres. The coordinates of the seed regions were extracted from previous literature devoted to the study of visual and motor functional pathways (51). This study confirmed that these seed locations are able to detect the modularity of the visual and motor cortices (represented as yellow and green dots in the brain graphs in **Fig. 3B**). A binary mask was created for each seed region, one mask containing the left hemisphere seeds: V1 and M1; and the other mask containing the right hemisphere seeds: V1 and M1. SFC identifies brain regions connected to specified seed regions (*i.e.*, nodes) at different *step distances* (*i.e.*, links or edges), where the number of *steps* equals the number of edges needed for connecting one brain voxel to a target node (52). First, at the individual level and in a voxel-wise approach, the weighted degree of stepwise connectivity was calculated by summing the weight of edges from a given single brain voxel to both seed regions (left V1-M1 or right V1-M1). The edges included were those with a length of

one-link step (*i.e.*, a direct connection) or a length of two-link steps (*i.e.*, an indirect connection) (see small diagram in bottom-right of **Fig. 3B**).

Direct connectivity for voxel *i* was computed as:

$$DC(i) = \sum_s FC(s,i)$$

where FC is the FDR thresholded functional connectivity matrix (FDR corrected), and *s* is each voxel within each seed mask.

Indirect connectivity for voxel *i* was computed as:

$$IC(i) = \frac{\sum_s \sum_{j=1}^{n} FC(s,j) * FC(j,i)}{\max\,(FC * FC)}$$

where *n* is the number of voxels in the brain.

Second, the connectivity degree of all one- and two-link step distances was calculated and set aside as interconnector SFC matrices, which expressed the total number of direct and indirect [at two steps] links from each interconnector node to V1 and M1. The direct interconnector SFC matrix was computed as:

$$IDC(i,j) = \sum_s FC(i,s)FC(s,j)$$

And, the indirect interconnector SFC matrix was computed as:

$$IIC(i,j) = \frac{\sum_s (\sum_{k=1}^{n} FC(i,k) * FC(k,s)\ \sum_{l=1}^{n} FC(s,l) * FC(l,j)\ )}{\max\,(FC * FC)}$$

Finally, the *mean interconnector map* was computed using the normalized z-score version, using the following equations:

Normalized direct interconnector map $DI(i) = \frac{\left(\sum_{j=1}^{n} IDC(i,j)\right) - m}{\mathrm{s}}$

where $m = \frac{\sum_{i=1}^{n}\sum_{j=1}^{n} IDC(i,j)}{\mathrm{n}}$ and $s = \sqrt{\frac{\sum_{i=1}^{n}(\sum_{j=1}^{n} IDC(i,j) - m)^2}{\mathrm{n}}}$

Normalized indirect interconnector map $II(i) = \frac{\left(\sum_{j=1}^{n} IIC(i,j)\right) - m}{\mathrm{s}}$

where $m = \frac{\sum_{i=1}^{n}\sum_{j=1}^{n} IIC(i,j)}{\mathrm{n}}$ and $s = \sqrt{\frac{\sum_{i=1}^{n}(\sum_{j=1}^{n} IIC(i,j) - m)^2}{\mathrm{n}}}$

From this analysis, two interconnector SFC maps were obtained for each data set (task or resting-state): one for left V1-M1 and one for right V1-M1. This analytical strategy determined the nodal interconnectors that link V1 and M1 in the entire cortex in the task and rest connectivity data. A final consensus *visuo-motor integration network*

map was obtained by calculating the mean map of the normalized task-activation map, task-connectivity SFC map, and rest-connectivity SFC map.

Combination of Neuroimaging and Allen Human Brain Atlas

Spatial Similarity Analysis. We used the Allen Human Brain Atlas (AHBA) to investigate the spatial similarities between protein-coding genetic profiles and our VMI consensus map (**Fig. 3C** and **D**). The AHBA provides whole-brain genome-wide expression patterns for six human subjects (85). For the spatial similarity strategy, we used the surface anatomical transformation of the transcription profiles, which includes 20,737 protein-coding genes, based on 58,692 measurements of gene expression in 3,702 brain samples obtained from those 6 adult human subjects (86). The surface anatomical transformation is based on the 68 cortical regions of the Desikan-Killiany atlas (87), which covers the entire cortex and uses individual vectors of the median cortical expression of the genes across the 68 cortical regions (**Fig. 3C**). The spatial similarity analysis was done by means of Matlab in-house developed coding (Matlab R2015b, Natick, Massachusetts: The MathWorks Inc.). The aim of the spatial similarity analysis was to find which genes, from the 20,737 genes of the AHBA, had a cortical expression that matched the brain regions identified in the VMI network map. We built a null hypothesis distribution by comparing the entire transcriptome with the VMI network map. Then, we detected which genes conferring risk for specific neuro-genetic syndromes surpassed a significant spatial correlation value in the upper-tail of the null hypothesis distribution (threshold of *r-value* > 1.96 standard deviations; red area in **Fig. 3D**). The *a priori* neurodevelopmental syndromes studied were: ASD, Dravet, Fragile-X, Prader-Willi, Turner and Williams. An individual list of the chromosomes impaired in each syndrome along with the genes selected (also called Visuo-Motor Syndromic Genes throughout the text; N=80) within the chromosomes for this study was based on GeneReviews (https://www.ncbi.nlm.nih.gov/books/NBK1116 as of June, 2018; ***SI* Appendix, Table S1**). Next, we used a resampling strategy to calculate the corrected *p*-value of each similarity comparison between specific genes and the VMI network map. We used Matlab's random permutation function and 1,000 iterations to probe if solid topological associations exist between targeted genes and the VMI map. The random permutation analysis was calculated over: (*i*) each gene's median cortical expression extracted from the Allen Human Brain Atlas across the 68 cortical regions included in the surface anatomical transformation based on the Desikan-Killiany atlas; (*ii*) the

visuo-motor integration network map data. Then, for each run of the resampling analysis, the Pearson product-moment correlation coefficient was calculated between the abovementioned variables. Finally, a probability distribution with the results of the resampling analysis was computed for each gene. The statistical significance of spatial VMI and genetic similarity score of each individual gene was corrected using a FDR approach (84); a $q<0.001$ FDR correction was applied to the *p-values* matrix; **Fig. 1** and ***SI Appendix*, Fig. S1**). As a complementary strategy, we tested whether the probability of our correlation values obtained between the genes and the consensus map were due to chance. We generated 1,000 random maps based on the same spatial smoothing level as the one in the consensus map. Then, we obtained the null hypothesis distribution of similarity scores with these random maps and corrected all p-values with a FDR approach (**SI Appendix, Fig. S2**).

Biological Processes of Genes Mediating Visuo-Motor Integration. The list of genes whose spatial cortical expression demonstrated high spatial correlation with the VMI network was entered in a Gene Ontology (GO) term enrichment analysis tool (http://geneontology.org; ref. 88). GO is a genetic annotation resource dedicated to investigating gene functionalities. In the present research, we used the annotation systems of *biological processes and cellular components* within GO to characterize our findings. *Biological Processes* are focused on "biological programs accomplished by multiple molecular activities" (88), that is, gene actions that lead to specific objectives, which are done under regulated procedures and temporal sequences. *Cellular Components* are focused on "the locations relative to cellular structures in which a gene product performs a function" (88). We computed a *Protein Analysis Through Evolutionary Relationships (PANTHER) Overrepresentation Test* (21) within the *term enrichment analysis* tool of the GO resource using the list of genes whose spatial cortical expression demonstrated high spatial correlation with the VMI network. The PANTHER resource classifies protein sequences of genes in terms of their evolutionary history and function; making it possible to formulate inferences about these gene functions [(a detailed description of PANTHER is available on (21)]. During the PANTHER Overrepresentation Test, the *Homo Sapiens* list (with all the genes included in the database) was selected as the reference list and the *GO Biological Processes* and *Cellular Components* were selected as the annotation data sets. A binomial test was then conducted ($p<0.05$ FDR-corrected) for each annotation data set. The results of the

analysis were based on their relative term enrichment, which represents to what extent each annotation is statistically represented in a set of given genes.

Interactome Analysis. Using an interactome approach, we validated our genetic findings beyond their spatial co-localizations with the VMI cortical map. We used Genemania [http://www.genemania.org; (ref. 89)] and Cytoscape [www.cytoscape.org; (ref. 90)] software to perform an interactome analysis and degree centrality assessment of the set of genes obtained in the Spatial Similarity Analysis. We used the Genemania's composite gene-gene interaction profile from co-expressions, co-localizations, genetic interactions, pathways, predicted physical interactions, and shared protein domains (89).

Materials, data and code availability

Neuroimaging data

The neuroimaging dataset acquired during the task-MRI paradigm is available from the corresponding author (J.S. sepulcre@nmr.mgh.harvard.edu) upon request, and the dataset acquired during the resting-state MRI paradigm from the Human Connectome Project website (https://www.humanconnectomeproject.org).

Genetic data

The genetic data that supports the findings of this study is available from the Allen Human Brain Atlas website (https://human.brain-map.org).

Code availability

All codes for imaging analysis are available for the research community from the corresponding author (J.S. sepulcre@nmr.mgh.harvard.edu) upon request.

References

1. C. Dravet, H. Oguni, “Dravet syndrome (severe myoclonic epilepsy in infancy)” in Handbook of Clinical Neurology, O. Dulac, M. Lassonde, H. B. Sarnat, Eds. (Elsevier, 2013), pp. 627–633 https://doi.org/10.1016/B978-0-444-52891-9.00065-8

2. D. Chieffo, et al., Neuropsychological development in children with Dravet syndrome. *Epilepsy Res.* **95**, 86–93 (2011) https://doi.org/10.1016/j.eplepsyres.2011.03.005

3. M. Wolff, C. Cassé-Perrot, C. Dravet, Severe myoclonic epilepsy of infants (Dravet syndrome): natural history and neuropsychological findings. *Epilepsia*. **47 Suppl 2**, 45–48 (2006) https://doi.org/10.1111/j.1528-1167.2006.00688.x

4. M. Borodyanskaya, S. Coffey, M. Y. Ono, R. J. Hagerman, “Intergenerational effects of mutations in the fragile X mental retardation 1 gene. Fragile X: A model of X-linked mental retardation and neurodegeneration” in Genes, Brain, and Development, M. A. Barnes, Ed. (Cambridge University Press, 2010), pp. 3–18 https://doi.org/10.1017/CBO9780511770708.002

5. J. Whittington, A. Holland, Cognition in people with Prader-Willi syndrome: Insights into genetic influences on cognitive and social development. *Neurosci. Biobehav. Rev.* **72**, 153–167 (2017) https://doi.org/10.1016/j.neubiorev.2016.09.013

6. S. T. Lo, P. J. L. Collin, A. C. S. Hokken-Koelega, Visual-motor integration in children with Prader-Willi syndrome. *J. Intellect. Disabil. Res.* **59**, 827–834 (2015) https://doi.org/10.1111/jir.12197

7. L. Reus, L. A. van Vlimmeren, J. B. Staal, B. J. Otten, M. W. G. Nijhuis-van der Sanden, The effect of growth hormone treatment or physical training on motor performance in Prader-Willi syndrome: a systematic review. *Neurosci. Biobehav. Rev.* **36**, 1817–1838 (2012) https://doi.org/10.1016/j.neubiorev.2012.05.005

8. J. Rovet, Turner syndrome: a review of genetic and hormonal influences on neuropsychological functioning. *Child. Neuropsychol.* **10**, 262–279 (2004) https://doi.org/10.1080/09297040490909297

9. M. W. G. Nijhuis-van der Sanden, P. A. T. M. Eling, B. J. Otten, A review of neuropsychological and motor studies in Turner Syndrome. *Neurosci. Biobehav. Rev.* **27**, 329–338 (2003) https:// doi.org/10.1016/s0149-7634(03)00062-9

10. L. J. Lewandowski, Clinical syndromes among the learning disabled. *J. Learn. Disabil.* **18**, 177–178 (1985) https://doi.org/10.1177/002221948501800316

11. J. Atkinson, The Davida Teller Award Lecture, 2016: Visual Brain Development: A review of "Dorsal Stream Vulnerability"-motion, mathematics, amblyopia, actions, and attention. *J. Vis.* **17**, 26 (2017) https://doi.org/10.1167/17.3.26

12. C. A. Morris, "Williams Syndrome" in GeneReviews® [Internet], M. P. Adam, H. H. Ardinger, R. A. Pagon et al., Eds. (Seattle, WA: University of Washington, 199 – Updated 2017) Available from: https://www.ncbi.nlm.nih.gov/books/NBK1249/

13. M. Miller, L. Chukoskie, M. Zinni, J. Townsend, D. Trauner. Dyspraxia, motor function and visual–motor integration in autism. *Behav. Brain. Res.* **269,** 95–102 (2014) https://doi.org/10.1016/j.bbr.2014.04.011

14. K. A. Fournier, C. J. Hass, S. K. Naik, N. Lodha, J. H. Cauraugh, Motor Coordination in Autism Spectrum Disorders: A Synthesis and Meta-Analysis. *J. Autism Dev. Disord.* **40**, 1227–1240 (2010) https://doi.org/10.1007/s10803-010-0981-3

15. H. Memisevic, M. Djordjevic, Visual-Motor Integration in Children with Mild Intellectual Disability: A Meta-Analysis. *Percept. Mot. Skills.* **125**, 696–717 (2018) https://doi.org/10.1177/0031512518774137

16. K. E. Beery, N. A. Beery, "Beery VMI: The Beery-Buktenica developmental test of visual-motor integration with supplemental developmental tests of visual perception and motor coordination and stepping stones age norms from birth to age six. Administration, scoring, and teaching manual" (New York, NY: PsychCorp, 2010)

17. B. Wiśniowiecka-Kowalnik, B. A. Nowakowska, Genetics and epigenetics of autism spectrum disorder—current evidence in the field. *J. Appl. Genet.* **60**, 37–47 (2019) https://doi.org/10.1007/s13353-018-00480-w

18. T. N. Turner et al., Genome Sequencing of Autism-Affected Families Reveals Disruption of Putative Noncoding Regulatory DNA. *Am. J. Hum. Genet.* **98**, 58–74 (2016) https://doi.org/10.1016/j.ajhg.2015.11.023

19. E. M. Dykens, E. Lee, E. Roof, Prader–Willi syndrome and autism spectrum disorders: an evolving story. *J. Neurodev. Disord.* **3**, 225–237 (2011) https://doi.org/10.1007/s11689-011-9092-5

20. E. H. Shen, C. C. Overly, A. R. Jones, The Allen Human Brain Atlas. *Trends. Neurosci.* **35**, 711–714 (2012) https://doi.org/10.1016/j.tins.2012.09.005

21. H. Mi, et al., PANTHER version 11: expanded annotation data from Gene Ontology and Reactome pathways, and data analysis tool enhancements. *Nucleic. Acids. Res.* **45**, D183–D189 (2017) https://doi.org/10.1093/nar/gkw1138

22. R. R. Green, et al., Beery VMI performance in autism spectrum disorder. Child Neuropsychol. *Child. Neuropsychol.* **22**, 795–817 (2016) https://doi.org/10.1080/09297049.2015.1056131

23. C. Cassé-Perrot, M. Wolff, C. Dravet, "Neuropsychological Aspects of Severe Myoclonic Epilepsy in Infancy" in Neuropsychology of Childhood Epilepsy. Advances in Behavioral Biology I. Jambaqué, M. Lassonde, O. Dulac, Eds. (Springer, 2001) vol. 50, pp. 131–140 https://doi.org/10.1007/0-306-47612-6_14

24. R. T. Schultz, et al., Visual–motor integration functioning in children with Tourette syndrome. *Neuropsychology.* **12,** 134–145 (1998) https://doi.org/10.1037/0894-4105.12.1.134

25. A. Herwig, Linking perception and action by structure or process? Toward an integrative perspective. *Neurosci. Biobehav. Rev.* **52**, 105–116 (2015) https://doi.org/10.1016/j.neubiorev.2015.02.013

26. G. Erdogan, Q. Chen, F. E. Garcea, B. Z. Mahon, R. A. Jacobs, Multisensory Part-based Representations of Objects in Human Lateral Occipital Cortex. *J. Cogn. Neurosci.* **28**, 869–881 (2016) https://doi.org/10.1162/jocn_a_00937

27. M. J. Naumer, et al., Visuohaptic convergence in a corticocerebellar network. *Euro. J. Neurosci.* **31**, 1730–1736 (2010) https://doi.org/10.1111/j.1460-9568.2010.07208.x

28. T. W. James, et al., Haptic study of three-dimensional objects activates extrastriate visual areas. *Neuropsychologia*. **40**, 1706–1714 (2002) https://doi.org/10.1016/s0028-3932(02)00017-9

29. A. Amedi, R. Malach, T. Hendler, S. Peled, E. Zohary, Visuo-haptic object-related activation in the ventral visual pathway. *Nat. Neurosci.* **4**, 324–330 (2001) https://doi.org/10.1038/85201

30. U. Halsband, R. K. Lange, Motor learning in man: A review of functional and clinical studies. *J. Physiol. Paris.* **99**, 414–424 (2006) https://doi.org/10.1016/j.jphysparis.2006.03.007

31. G. Rizzolatti, D. M. Wolpert, Motor systems. *Curr. Opin. Neurobiol.* **15**, 623–625 (2005) https://doi.org/10.1016/j.conb.2005.10.018

32. G. Gentile, V. I. Petkova, H. H. Ehrsson, Integration of Visual and Tactile Signals from the Hand in the Human Brain: An fMRI Study. *J. Neurophysiol.* **105**, 910–922 (2011) https://doi.org/10.1152/jn.00840.2010

33. E. Wacker, B. Spitzer, R. Lützkendorf, J. Bernarding, F. Blankenburg.Tactile Motion and Pattern Processing Assessed with High-Field fMRI. *PLoS. One.* **6**, e24860 (2011) https://doi.org/10.1371/journal.pone.0024860

34. S. B. Eickhoff, et al., Anatomical and Functional Connectivity of Cytoarchitectonic Areas within the Human Parietal Operculum. *J. Neurosci.* **30**, 6409–6421 (2010) https://doi.org/10.1523/jneurosci.5664-09.2010

35. J. P. Young, et al., Somatotopy and Attentional Modulation of the Human Parietal and Opercular Regions. *J. Neurosci.* **24**, 5391–5399 (2004) https://doi.org/10.1523/jneurosci.4030-03.2004

36. S. Vahdat, M. Darainy, T. E. Milner, D. J. Ostry. Functionally Specific Changes in Resting-State Sensorimotor Networks after Motor Learning. *J. Neurosci.* **31**, 16907–16915 (2011) https://doi.org/10.1523/jneurosci.2737-11.2011

37. B. Pleger, et al., Pharmacological suppression of plastic changes in human primary somatosensory cortex after motor learning. *Exp. Brain. Res.* **148**, 525–532 (2003) https://doi.org/10.1007/s00221-002-1324-1

38. G. J. Zelinsky, J. W. Bisley, The what, where, and why of priority maps and their interactions with visual working memory. *Ann. N. Y. Acad. Sci.* **1339**, 154–164 (2015) https://doi.org/10.1111/nyas.12606

39. F. Katsuki, C. Constantinidis, Bottom-Up and Top-Down Attention. *Neuroscientist.* **20**, 509–521 (2013) https://doi.org/10.1177/1073858413514136

40. R. J. Krauzlis, L. P. Lovejoy, A. Zénon, Superior Colliculus and Visual Spatial Attention. *Annu. Rev. Neurosci.* **36**, 165–182 (2013) https://doi.org/10.1146/annurev-neuro-062012-170249

41. J. W. Bisley, M. E. Goldberg, Attention, Intention, and Priority in the Parietal Lobe. *Annu. Rev. Neurosci.* **33**, 1–21 (2010) https://doi.org/10.1146/annurev-neuro-060909-152823

42. J. T. Serences, S. Yantis, Selective visual attention and perceptual coherence. *Trends. Neurosci.* **10**, 38–45 (2006) https://doi.org/10.1016/j.tics.2005.11.008

43. G. Deco, E. T. Rolls, Neurodynamical cortical model of visual attention and invariant object recognition. *Vision. Res.* **44**, 621–642 (2004) https://doi.org/10.1016/j.visres.2003.09.037

44. J. C. Culham, K. F. Valyear, Human parietal cortex in action. *Curr. Opin. Neurobiol.*, **16**, 205–212 (2006) https://doi.org/10.1016/j.conb.2006.03.005

45. R. M. de Azevedo Neto, E. Amaro Júnior, Bilateral dorsal fronto-parietal areas are associated with integration of visual motion information and timed motor action. *Behav. Brain. Res.* **337**, 91–98 (2018) https://doi.org/10.1016/j.bbr.2017.09.046

46. L. Ungerleider, M. Mishkin, "Two cortical visual systems" in The analysis of visual behaviour D. Ingle, M. A. Goodale, R. J. W. Mansfield, Eds. (MIT Press, 1982) pp. 549–586. Retrieved from https://mitpress.mit.edu/books/analysis-visual-behavior

47. G. Rizzolatti, L. Craighero, The mirror-neuron system. *Annu. Rev. Neurosci.* **27**, 169–192 (2004) https://doi.org/10.1146/annurev.neuro.27.070203.144230

48. A. Battaglia-Mayer, R. Caminiti, "Parieto-frontal networks for eye–hand coordination and movements" in Handbook of Clinical Neurology, G. Vallar, H Branch

Colsett, Eds. (Elsevier, 2018), vol. 151 pp. 499–524. https://doi.org/10.1016/B978-0-444-63622-5.00026-7

49. G. Rizzolatti, S. Rozzi, “The mirror mechanism in the parietal lobe” in Handbook of Clinical Neurology, G. Vallar, H Branch Colsett, Eds. (Elsevier, 2018), vol. 151 pp. 499–524https://doi.org/10.1016/B978-0-444-63622-5.00028-0

50. G. Rizzolatti, C. Sinigaglia, The functional role of the parieto-frontal mirror circuit: interpretations and misinterpretations. *Nat. Rev. Neurosci.* **11**, 264–274 (2010) https://doi.org/10.1038/nrn2805

51. J. Sepulcre, Functional Streams and Cortical Integration in the Human Brain. *Neuroscientist*. **20**, 499–508 (2014) https://doi.org/10.1177/1073858414531657

52. J. Sepulcre, M. R. Sabuncu, T. B., Yeo, H. Liu, K. A. Johnson, Stepwise connectivity of the modal cortex reveals the multimodal organization of the human brain. *J. Neurosci*, **32**, 10649–10661 (2012) https://doi.org/10.1523/JNEUROSCI.0759-12.2012

53. H. C. Chuang, T. N. Huang, Y. P. Hsueh, T-Brain-1 - A Potential Master Regulator in Autism Spectrum Disorders. *Autism. Res.* **8**, 412–426 (2015) https://doi.org/10.1002/aur.1456

54. C. P. Schaaf, et al., Truncating mutations of MAGEL2 cause Prader-Willi phenotypes and autism. *Nat. Gen.* **45**, 1405–1409 (2013) https://doi.org/10.1038/ng.2776

55. I. Ohmori, et al., CACNA1A variants may modify the epileptic phenotype of Dravet syndrome. *Neurobiol. Dis.* **50**, 209–217 (2013) https://doi.org/10.1016/j.nbd.2012.10.016

56. C. Dravet, The core Dravet syndrome phenotype. *Epilepsia*. **52**, 3–9 (2011) https://doi.org/10.1111/j.1528-1167.2011.02994.x

57. F. Guzzetta, Cognitive and behavioral characteristics of children with Dravet syndrome: An overview. *Epilepsia*. **52**, 35–38 (2011) https://doi.org/10.1111/j.1528-1167.2011.02999.x

58. I. Ohmori, et al., A CACNB4 mutation shows that altered Cav2.1 function may be a genetic modifier of severe myoclonic epilepsy in infancy. *Neurobil. Dis.* **32**, 349–354 (2008) https://doi.org/10.1016/j.nbd.2008.07.017

59. L. Claes, et al., De Novo Mutations in the Sodium-Channel Gene SCN1A Cause Severe Myoclonic Epilepsy of Infancy. *Am. J. Hum. Genet.* **68**, 1327–1332 (2001) https://doi.org/10.1086/320609

60. A. B. Mihalas, R. F. Hevner, Control of Neuronal Development by T-Box Genes in the Brain. *Curr. Top. Dev. Biol.* **122**, 279–312 (2017) https://doi.org/10.1016/bs.ctdb.2016.08.001

61. F. Bedogni, et al., Autism susceptibility candidate 2 (Auts2) encodes a nuclear protein expressed in developing brain regions implicated in autism neuropathology. *Gene. Expre. Patterns.* **10**, 9–15 (2010) https://doi.org/10.1016/J.GEP.2009.11.005

62. B. J. O'Roak, et al., Multiplex Targeted Sequencing Identifies Recurrently Mutated Genes in Autism Spectrum Disorders. *Science*. **338**, 1619–1622 (2012) https://doi.org/10.1126/science.1227764

63. S. D. Mayes, S. L. Calhoun, Learning, Attention, Writing, and Processing Speed in Typical Children and Children with ADHD, Autism, Anxiety, Depression, and Oppositional-Defiant Disorder. *Child Neuropsychol.* **13**, 469–493 (2007) https://doi.org/10.1080/09297040601112773

64. S. C. Fulkerson, W. M. Freeman. Perceptual-motor deficiency in autistic children. *Percept. Mot. Skills*. **50**, 331–336 (1980) https://doi.org/10.2466/pms.1980.50.1.331

65. R. Khalil, R. Tindle, T. Boraud, A. A. Moustafa, A. A. Karim, Social decision making in autism: On the impact of mirror neurons, motor control, and imitative behaviors. *CNS Neurosci. Ther.* **24**, 669–676 (2018) https://doi.org/10.1111/cns.13001

66. R. L. Moseley, F. Pulvermüller, What can autism teach us about the role of sensorimotor systems in higher cognition? New clues from studies on language, action semantics, and abstract emotional concept processing. *Cortex.* **100**, 149–190 (2018) https://doi.org/10.1016/j.cortex.2017.11.019

67. M. -J. Descheemaeker, V. Govers, P. Vermeulen, J.-P. Fryns, Pervasive developmental disorders in Prader-Willi syndrome: the Leuven experience in 59 subjects and controls. *Am. J. Med. Genet.* **140**, 1136–1142 (2006) https://doi.org/10.1002/ajmg.a.31235

68. I. Boccaccio, et al., The Human MAGEL2 Gene and Its Mouse Homologue Are Paternally Expressed and Mapped to the Prader-Willi Region. *Hum. Mol. Genet.* **8**, 2497–2505 (1999) https://doi.org/10.1093/hmg/8.13.2497

69. S. Bervini, H. Herzog, Mouse models of Prader-Willi Syndrome: a systematic review. *Front. Neuroendocrin.* **34**, 107–119 (2013) https://doi.org/10.1016/j.yfrne.2013.01.002

70. S. Lee, Expression and imprinting of MAGEL2 suggest a role in Prader-Willi syndrome and the homologous murine imprinting phenotype. *Hum. Mol. Genet.* **9**, 1813–1819 (2000) https://doi.org/10.1093/hmg/9.12.1813

71. J. Whittington, A. Holland, T. Webb, T, Relationship between the IQ of people with Prader-Willi syndrome and that of their siblings: evidence for imprinted gene effects. *J. Intellect. Disabil. Res.* **53**, 411–418 (2009) (2000) https://doi.org/10.1111/j.1365-2788.2009.01157.x

72. J. Jauregi et al., A neuropsychological assessment of frontal cognitive functions in Prader? Willi syndrome. *J. Intellect. Disabil. Res.* **51**, 350–365 (2007) https://doi.org/10.1111/j.1365-2788.2006.00883.x

73. A. Brunklaus, R. Ellis, E. Reavey, C. Semsarian, S. M. Zuberi, Genotype phenotype associations across the voltage-gated sodium channel family. *J. Med. Genet.* **51**, 650–658 (2014) https://doi.org/10.1136/jmedgenet-2014-102608

74. M. Oliva, S. F. Berkovic, S. Petrou. Sodium channels and the neurobiology of epilepsy. *Epilepsia*. **53**, 1849–1859 (2012) https://doi.org/10.1111/j.1528-1167.2012.03631.x

75. C. Marini, et al., The genetics of Dravet syndrome. *Epilepsia.* **52**, 24–29 (2011) https://doi.org/10.1111/j.1528-1167.2011.02997.x

76. A. Gambardella, C. Marini, Clinical spectrum of SCN1A mutations. *Epilepsia*. **50**, 20–23 (2009) https://doi.org/10.1111/j.1528-1167.2009.02115.x

77. C. E. Stafstrom, Severe Epilepsy Syndromes of Early Childhood: The Link Between Genetics and Pathophysiology with a Focus on SCN1A Mutations. *J. Child. Neurol.* **24**, 15S–23S (2009) https://doi.org/10.1177/0883073809338152

78. A. Escayg, et al., Mutations of SCN1A, encoding a neuronal sodium channel, in two families with GEFS+2. *Nat Genetics*. **24**, 343–345 (2000) https://doi.org/10.1038/74159

79. A. Escayg, A. L. Goldin, Sodium channel SCN1A and epilepsy: Mutations and mechanisms. *Epilepsia*. **51**, 1650–1658 (2010) https://doi.org/10.1111/j.1528-1167.2010.02640.x

80. R. C. Oldfield, The assessment and analysis of handedness: the Edinburgh inventory. *Neuropsychologia*. **9**, 97–113 (1971) Retrieved from http://www.ncbi.nlm.nih.gov/pubmed/5146491

81. A. J. Holmes, et al., Brain Genomics Superstruct Project initial data release with structural, functional, and behavioral measures. *Sci. Data.* **2**, 150031 (2015) https://doi.org/10.1038/sdata.2015.31

82. K. Murphy, R. M. Birn, D. A. Handwerker, T. B. Jones, P. A. Bandettini, The impact of global signal regression on resting state correlations: Are anti-correlated networks introduced? *Neuroimage*. **44**, 893–905 (2009) https://doi.org/10.1016/j.neuroimage.2008.09.036

83. K. R. A. Van Dijk, M. R. Sabuncu, R. L. Buckner, The influence of head motion on intrinsic functional connectivity MRI. *Neuroimage.* **59**, 431–438 (2012) https://doi.org/10.1016/j.neuroimage.2011.07.044

84. Y. Benjamini, D. Drai, G. Elmer, N. Kafkafi, I. Golani, Controlling the false discovery rate in behavior genetics research. *Behav. Brain. Res.* **125**, 279–284 (2001) Retrieved from http://www.ncbi.nlm.nih.gov/pubmed/11682119

85. M. J. Hawrylycz, et al., An anatomically comprehensive atlas of the adult human brain transcriptome. *Nature*. **489**, 391–399 (2012) https://doi.org/10.1038/nature11405

86. L. French, T. A. Paus, FreeSurfer view of the cortical transcriptome generated from the Allen Human Brain Atlas. *Front. Neurosci.* **9**, 323 (2015) https://doi.org/10.3389/fnins.2015.00323

87. R. S. Desikan, et al., An automated labeling system for subdividing the human cerebral cortex on MRI scans into gyral based regions of interest. *Neuroimage*. **31**, 968–980 (2006) https://doi.org/10.1016/j.neuroimage.2006.01.021

88. The Gene Ontology Consortium. Expansion of the Gene Ontology knowledgebase and resources. *Nucleic. Acids. Res.,* **45**, D331–D338 (2017) https://doi.org/10.1093/nar/gkw1108

89. S. Mostafavi, D. Ray, D. Warde-Farley, C. Grouios, Q Morris. GeneMANIA: a real-time multiple association network integration algorithm for predicting gene function. *Genome Biol.* **9**, S4 (2008) https://doi.org/10.1186/gb-2008-9-s1-s4

90. C. T. Lopes, et al., Cytoscape Web: an interactive web-based network browser. *Bioinformatics*, **26**, 2347–2348 (2010) https://doi.org/10.1093/bioinformatics/btq430

Figure legends

Figure 1. Neuroimaging-genetics results. (I) Three FDR-corrected source brain maps were used for determining the visuo-motor integration network. The top panel displays the task-fMRI activation results related to conducting group-level analysis of a finger-tapping task. The middle panel shows the task-functional connectivity results associated with the same finger-tapping task. The bottom panel shows the resting-state Functional Connectivity results of an independent sample. Each analysis result is displayed in left and right cortical hemispheric surfaces, with lateral and medial projections, and a clear brain colour scale (minimum=2% and maximum=98% threshold visualization). (II) Visuo-motor integrators. Left and right cortical hemispheric surfaces of the visuo-motor integration network map as a result of combining the three source brain maps (from I): *task activation*, *task connectivity* and *rest connectivity*. Letters mark the lateral occipital cortex (*a* and *d*), the OP4 (*c* and *f*) and the intraparietal sulcus (*b*, *e*, and black dotted line). Lateral, medial and flat projections were used in a clear brain colour scale (min=2% and max=98% threshold visualization). (III) Syndromic genes linked to the visuo-motor integration network. Left panel: the similarity distribution represents the results of the topographical similarity analysis between the visuo-motor integration network cortical map and the brain transcriptome map (cortical gene expression map of ~20,000 protein-coding genes). Genes with high cortical expression within the visuo-motor integration network have high similarity score (red dotted line above 1.96 standard deviations). Right panel: fold enrichment (FE) representation of the Gene Ontology biological profiles of the genes with high cortical expression within the visuo-motor integration network (FE>2; statistically significant FDR-corrected $q<0.05$). (IV) TBR1 gene and the VMI network. Bottom panel: scatterplot showing the topographical similarity relationship between the visuo-motor integration network map and the cortical gene expression of the TBR1 gene across the Desikan-Killiany atlas (linear fit=red dotted line). Top panel: null distribution of the topographical similarity based on a resampling random permutation approach. The red dotted arrow marks the similarity coefficient and the statistically significant *p-value* of the topographical similarity relationship between the visuo-motor integration network map and the cortical gene expression of the TBR1 gene. Figure abbreviations: L=left; R=right; min=minimum; max=maximum; SS=spatial similarity; VMI=visuo-motor integration.

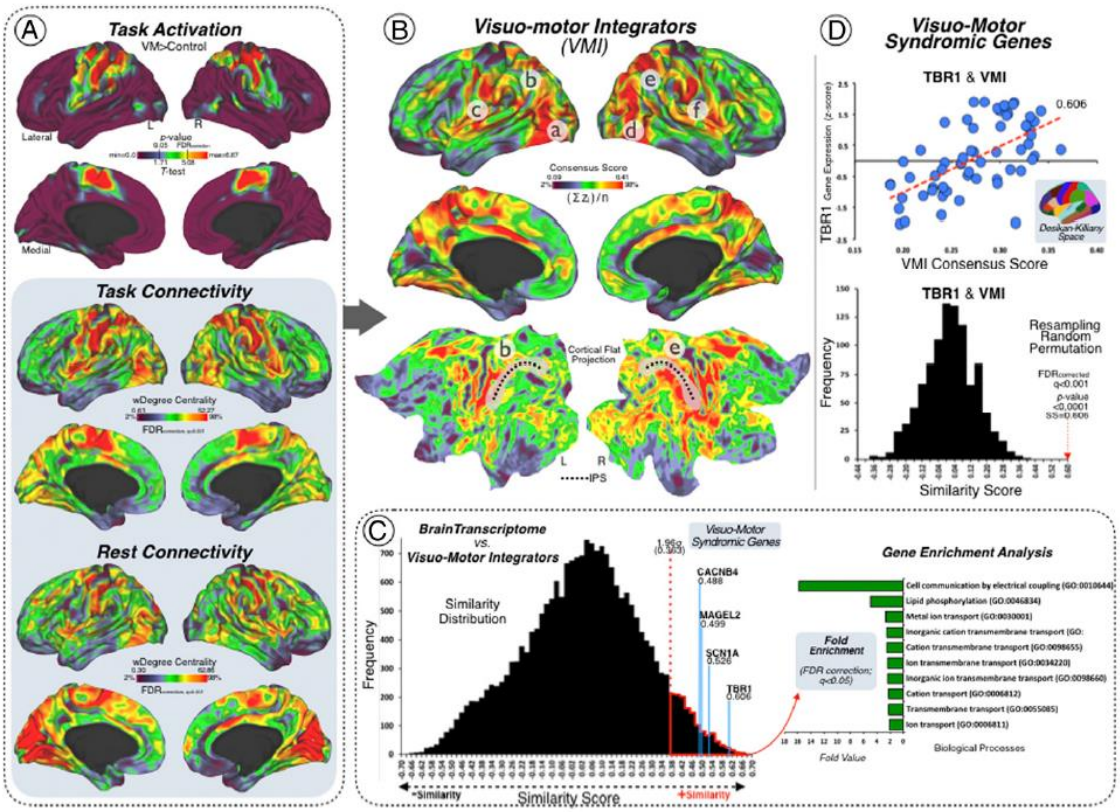
A
Task Activation
VM>Control
Lateral
Medial
L
R
p-value
T-test
Task Connectivity
wDegree Centrality
Rest Connectivity
wDegree Centrality
B
Visuo-motor Integrators
(VMI)
Consensus Score
(Σz)/n
Cortical Flat Projection
L
R
IPS
C
BrainTranscriptome
vs.
Visuo-Motor Integrators
Visuo-Motor Syndromic Genes
Similarity Distribution
Frequency
CACNB4
0.488
MAGEL2
0.499
SCN1A
0.526
TBR1
0.606
-Similarity
Similarity Score
+Similarity
Gene Enrichment Analysis
Fold Enrichment
(FDR correction; q<0.05)
Cell communication by electrical coupling (GO:0010644)
Lipid phosphorylation (GO:0046834)
Metal ion transport (GO:0030001)
Inorganic cation transmembrane transport (GO:
Cation transmembrane transport (GO:0098655)
Ion transmembrane transport (GO:0034220)
Inorganic ion transmembrane transport (GO:0098660)
Cation transport (GO:0006812)
Transmembrane transport (GO:0055085)
Ion transport (GO:0006811)
Fold Value
Biological Processes
D
Visuo-Motor
Syndromic Genes
TBR1 & VMI
TBR1 Gene Expression (z-score)
0.606
Desikan-Killiany Space
VMI Consensus Score
TBR1 & VMI
Resampling
Random
Permutation
Frequency
Similarity Score

1

2

Figure 2. Genetic network analysis. (I) The protein-coding genes from the Allen Human Brain Atlas with high cortical expression within the visuo-motor integration network (above 1.96 standard deviations) are displayed in the network topological space. (II) The genes are plotted as a function of the network's degree centrality. The genes related to neurodevelopmental disorders are highlighted in matching colours in (I) and (II). TBR1 gene is represented in red colour and the other three syndromic genes – CACNB4, MAGEL2 and SCN1A – are represented in darker to lighter blue tones.

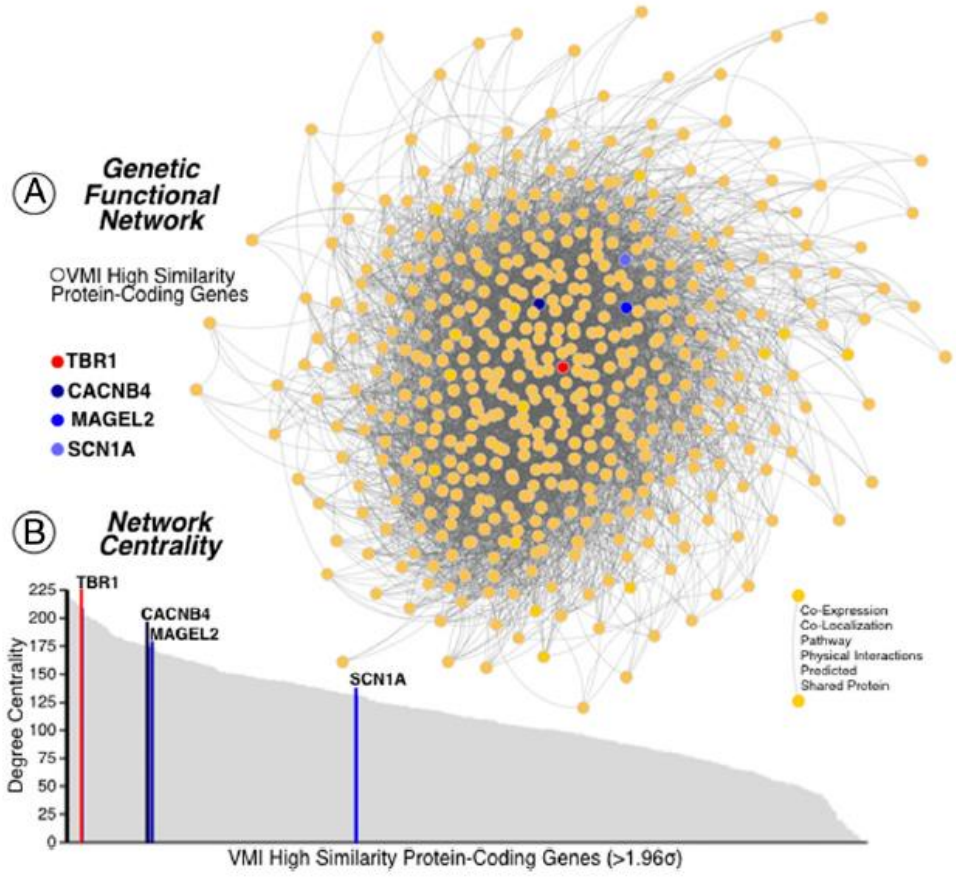

1

Figure 3. Pipeline overview. (I) Neuroimaging data. Functional MRI blood oxygenation level-dependent (BOLD) data of the cerebral cortex was recorded at the voxel level for subsequent graph functional connectivity analysis at the node level. (II) Visuo-motor integration network. Degree centrality analysis was used to investigate the whole-brain functional connectivity of all brain nodes. Then, stepwise functional connectivity was used to investigate the connections departing from modal areas with the aim of discovering their intersection. Two modal areas were studied: the primary visual cortex (represented as yellow dots and as the modal network A) and the primary motor cortex (represented as green dots and as the modal network B). The method revealed the cortical areas supporting the integration of visual and motor information (represented as red dots and as the modal network C). Bottom panel: brain functional connectivity graphs derived from resting-state and task datasets were combined with a task-activation dataset for building the visuo-motor integration network cortical map. Task activation detects the activation changes throughout the cortex and functional connectivity points out the connections (links or paths) between cortical regions. (III) Brain genetics. Diagram of the genetic expression matrix for the 20,737 protein-coding genes from the Allen Human Brain Atlas, across the 68 brain cortical regions included in the surface anatomical transformation of the Desikan-Killiany atlas. The brain map allows investigating whole-brain transcriptome including the genetic expression levels of syndromic genes associated with visuo-motor functions. (IV) Neuroimaging-genetics relation. A topographical similarity analysis was done between the visuo-motor integration network cortical map and the cortical gene expression map of the syndromic genes. This analysis allows localizing the genes with high cortical expression within the visuo-motor integration network map (area of the histogram highlighted in red, corresponds to similarity scores above 1.96 standard deviations).

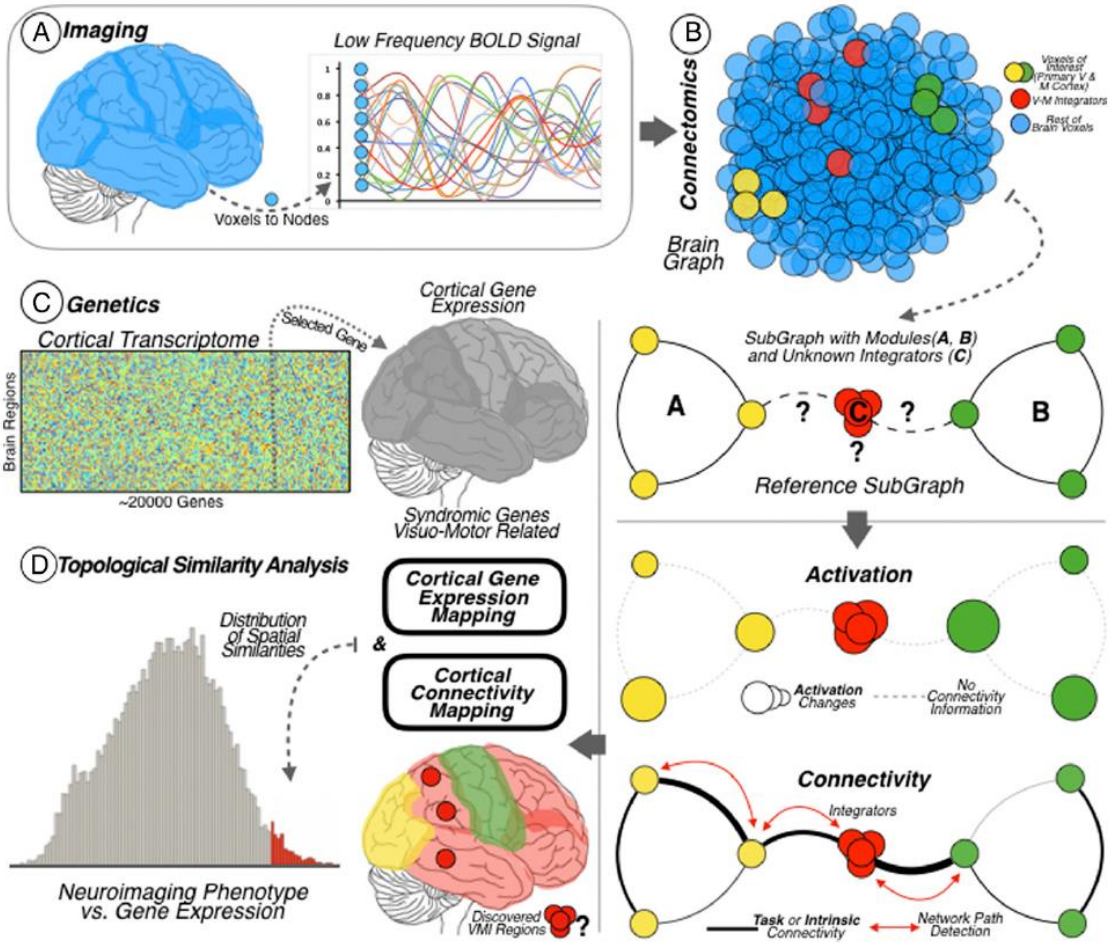
A Imaging
Low Frequency BOLD Signal
Voxels to Nodes
B
Connectomics
Brain Graph
Voxels of Interest (Primary V & M Cortex)
V-M Integrators
Rest of Brain Voxels
C Genetics
Cortical Transcriptome
Selected Gene
Brain Regions
~20000 Genes
Cortical Gene Expression
Syndromic Genes Visuo-Motor Related
SubGraph with Modules(A, B) and Unknown Integrators (C)
A
B
C
Reference SubGraph
D Topological Similarity Analysis
Distribution of Spatial Similarities
&
Cortical Gene Expression Mapping
Cortical Connectivity Mapping
Neuroimaging Phenotype vs. Gene Expression
Discovered VMI Regions
Activation
Activation Changes
No Connectivity Information
Connectivity
Integrators
Task or Intrinsic Connectivity
Network Path Detection

Supporting Information

Supporting information document for "***Central Neurogenetic Signatures of the Visuo-Motor Integration System***" by Bueichekú et al.

Correspondence should be addressed to:

Jorge Sepulcre (sepulcre@nmr.mgh.harvard.edu).

The document contains the following sections:

SI Methods

Visuo-Motor Integration Task Description

A finger-tapping task was used as the experimental task-MRI paradigm. The task consisted of learning a sequence of alternating finger movements. Colored circles assigned one to each finger were used to present the sequence of finger movements (color 1: little finger, color 2: ring finger; color 3: middle finger; and, color 4: index finger). First, the sequence of movements was presented on the screen at 0.67 Hz, followed by a fixation cross that remained for 12.5 seconds, allowing time for the participants to reproduce the sequence. Before each sequence, there was a random jitter (0-500 ms), the task had eight sequences of movements per condition and there were 4000 ms of rest after each sequence. There were two task conditions: 1) ordered sequence of movements, where the participants performed the following movements: 1-2-3-4-1-2-3-4; and, 2) alternating sequence of movements where the participants performed novel sequences. The sequences were performed with the right hand, the left hand and bimanually; the hand condition was counterbalanced across participants. The bimanual performance required symmetrical simultaneous movements. Feedback was not provided during the task performance or after it. For the purpose of the present investigation, only the data related to the ordered sequence of movements and the bimanual performance were used.

Data Acquisition Details

MRI data from Cohort 1 were acquired on a 3.0 T Siemens TIM Trio scanner (Siemens Healthcare, Erlangen, Germany) using an 8-channel head coil. The acquisitions covered the whole brain including the entire cerebellum. Firstly, a high-resolution T1-weighted magnetization-prepared rapid acquisition gradient echo (MPRAGE) images were acquired as structural data (repetition time / echo time [TR/TE] =1620 / 3.09 ms, flip angle=15º, 1 mm^3 isotropic voxels, 160 slices). Then, T2-weighted gradient echo echo-planar imaging (EPI) sequences sensitive to blood oxygenation level-dependent (BOLD) contrast (TR/TE = 3000/30ms, flip angle = 90º, 3 mm^3 isotropic voxels, no inter-slice gap, 49 slices) were used to acquire 244 volumes for each task run (right hand run, left hand run, and bimanual run).

Stimuli presentation and response collection was controlled using Cogent (Cogent 2000, UCL, London) and Matlab software (MATLAB R2010a, Natick, Massachusetts:

The MathWorks Inc.), which was installed in a fixed workstation (screen-resolution 1080p, refresh rate of 67 Hz). Images were projected onto a screen and then reflected by a mirror system attached to the head coil into the subjects' field of vision and their responses were collected by two 4-key response pads (Current Designs, Inc.), one for each hand.

According to (1), Cohort 2 images were acquired on a 3.0 T Siemens TIM Trio scanner (Siemens Healthcare, Erlangen, Germany) at Harvard University and the Massachusetts General Hospital using a 12-channel phased-array head coil. The acquisitions covered the whole brain including the entire cerebellum. Slices were aligned to the AC-PC plane. Firstly, a high-resolution T1-weighted multi-echo MPRAGE images were acquired as structural data (TR=2.2 ms, TE= 1.5/3.4/5.2/7.0 ms, flip angle = 7º, 1.2 mm^3 isotropic voxels, 144 slices). Then, functional images corresponding to the resting-state scan were acquired using a gradient-echo EPI sequence sensitive to BOLD contrast (TR / TE = 3000 / 30 ms, flip angle = 85º, 3 mm^3 isotropic voxels, 124 volumes). For resting-state scans, participants were instructed to stay awake and still, with their eyes open and blinking normally.

Image Preprocessing

The four initial data time points of the BOLD acquisitions were discarded from the analysis to allow for signal stabilization. As abovementioned, for task activation analysis (from Cohort 1) only the data related to the ordered sequence of movements and the bimanual performance was used, thus, 120 data time points were analyzed. The set of images were preprocessed using Statistical Parametrical Mapping 12 software (SPM12, Wellcome Department of Imaging Neuroscience, London, England; www.fil.ion.ucl.ac.uk/spm/). Standard preprocessing was conducted, which included the following steps: (*i*) the correction of the slice timing differences for interleaved ascending acquisitions (using the middle slice, which was the 49^{th}, as the reference slice); (*ii*) two-pass procedure in realignment (registered to the first image, and then registered to the mean image) to correct for head motion during acquisition, no head motion for any participant's data had more than 2.0 mm of maximum displacement in any direction, or 2.0° of any angular motion; (*iii*) spatial normalization to Montreal Neurological Institute (MNI) space (3 mm^3 isotropic), which was conducted using the mean resliced image as source and the EPI provided by SPM12 as the template; (i*v*)

spatial smoothing using an isotropic Gaussian kernel of 6 mm^3 full-width at half-maximum (FWHM).

For functional connectivity analysis, task related functional images from Cohort 1 and resting-state functional images from Cohort 2 were independently preprocessed, but the same procedure was used to obtain low-frequency fluctuations of BOLD signal (**Fig. 3A**). As for the task-activation analysis, for functional connectivity analyses 120 data time points were analyzed, discarding the initial four BOLD volumes. Each set of images was processed using a custom in-house developed preprocessing pipeline. The preprocessing included the following steps: (*i*) slice timing acquisition correction for interleaved ascending acquisitions (using the middle slice as the reference); (*ii*) two pass procedure in realignment (first registration to the first image, then registration to the mean image); (*iii*) intensity normalization; (*iv*) nuisance covariate regression which included signal detrending (lineal and quadratic trends), applying the Friston 24-parameter model as a head motion regression model (signal regression of six parameters from rigid body head motion obtained from realignment step and their temporal derivative, followed by the quadratic conversion of all 12 variables), and applying the component based method CompCorr for the reduction of noise (with 5 parameters for cerebrospinal fluid signal and 5 parameters for white matter signal); (*v*) normalization to the MNI space (3 mm^3 isotropic); (*vi*) band-pass filtering retaining BOLD signal between 0.01 Hz and 0.08 Hz; (*vii*) data demeaning with mean centered to 0; (*viii*) data motion-censoring step (*i.e.*, scrubbing of the time points with excess motion) was performed through interpolation according to (2), with the frame displacement (FD) threshold set to FD > 0.5 mm, none of the participants had excessive head motion; (*ix*) finally, for computational efficiency, the data were down-sampled from 3 mm^3 to 6 mm^3 voxel size.

SI Figures

Figure S1. Bootstrap resampling approach (I). Resampling-based similarity scores histograms of syndromic genes - SCN1A, MAGEL2 and CACNB4 - with genetic expression highly associated with the VMI map (using each gene's median cortical expression for the bootstrap resampling analysis). All relevant neuroimaging-genetic associations remained statistically significant after FDR correction.

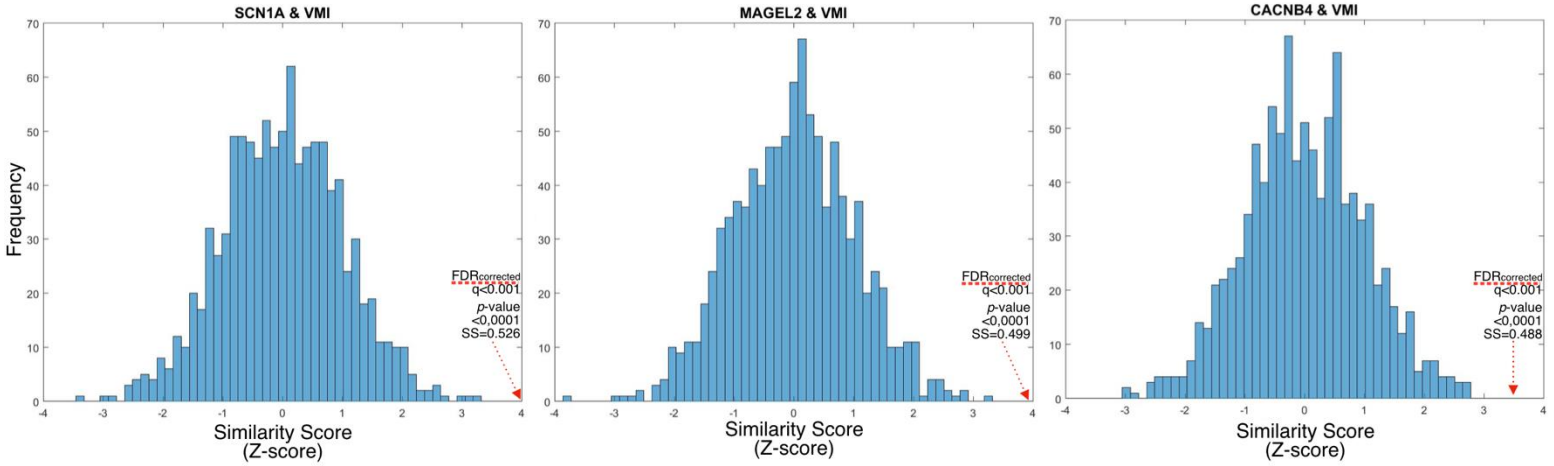

Figure S2. Bootstrap resampling approach (II). Resampling-based similarity scores histograms of syndromic genes - TBR1, SCN1A, MAGEL2 and CACNB4 - with genetic expression highly associated with the VMI map (using random maps for the bootstrap resampling analysis). All relevant neuroimaging-genetic associations remained statistically significant after FDR correction.

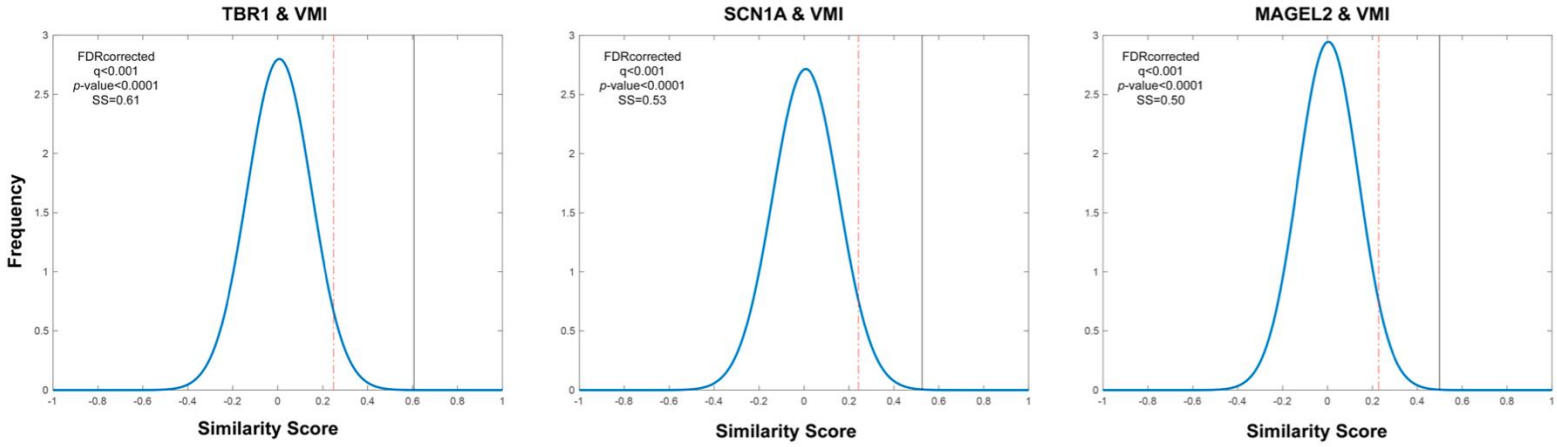

Figure S3. Gene expression levels of VMI-related genes. Cortical topology in the Desikan-Killiany atlas space of gene expression levels of TBR1 (top-left), SCN1A (top-right), MAGEL2 (bottom-left), and CACNB4 (bottom-right). Color scale represents the Allen Human Brain Atlas scores of gene transcripts (minimum = 2% and maximum = 98%).

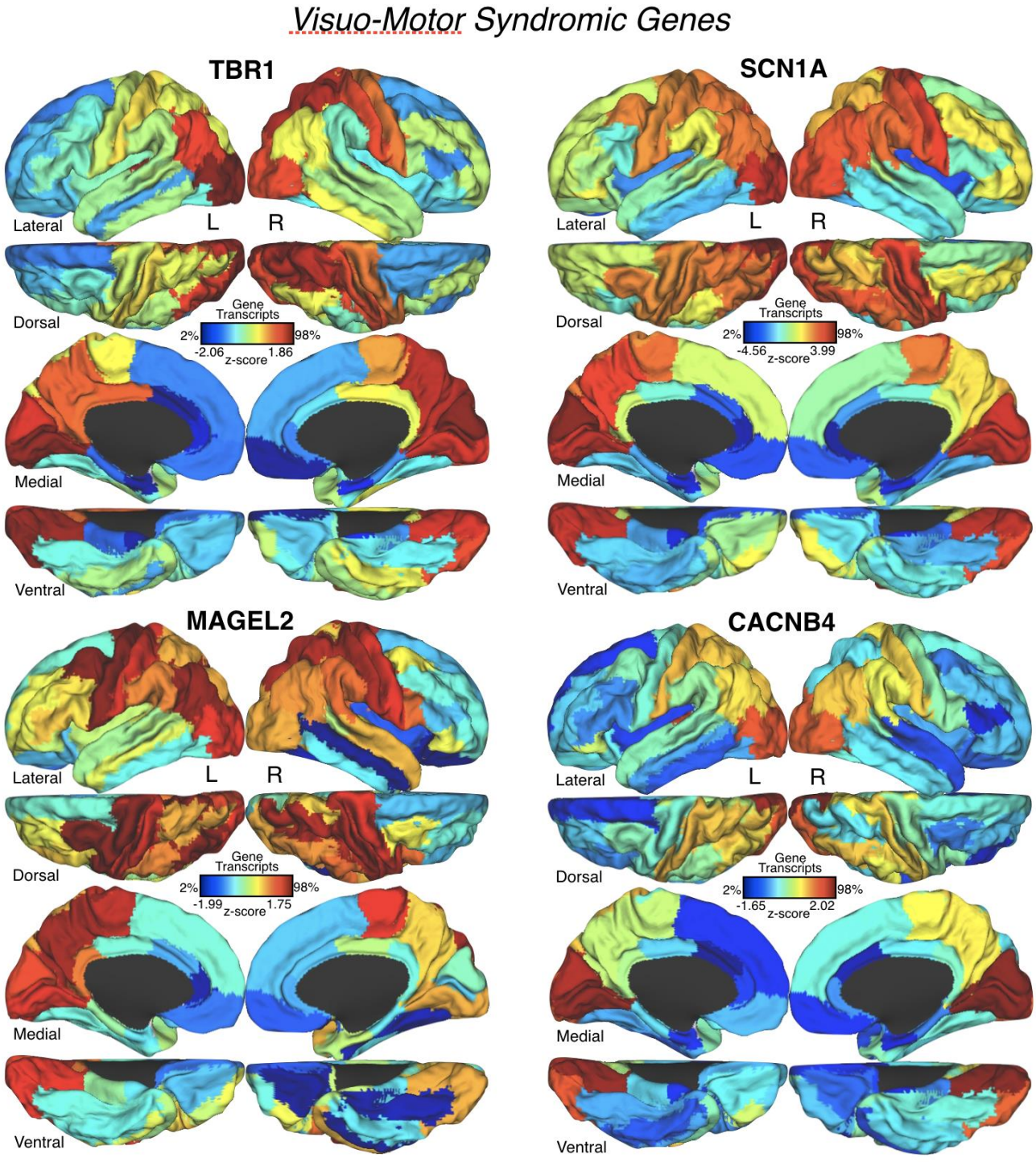

SI Tables

Table S1. List of genes associated with neurodevelopmental syndromes. The GeneReviews resource was used for searching the chromosomes impaired in each syndrome, along with genes affected within those chromosomes (N=80).

Autism Spectrum Disorder	Dravet Syndrome	Fragile-X Syndrome	Prader-Willi Syndrome	Turner Syndrome	Williams Syndrome
ADNP	CACNA1A	FMR1	ATP10A	SHOX	ABHD11
ANK2	CACNB4		BP3		BAZ1B
ARID1B	POLG		GABRA5		BCL7B
ASH1L	SCN1A		GABRB3		CLDN3
ASXL3	SCN9A		GABRG3		CLDN4
CHD8			GCP5		CLIP2
CUL3			HERC2		DNAJC30
DSCAM			MAGEL2		EIF4H
DYRK1A			MKRN3		ELN
GRIN2B			NDN		FKBP6
KATNAL2			NECDIN		FZD9
KMT2A			NIPA1		GTF2I
KMT5B			NIPA2		GTF2IRD1
MYT1L			NPAP1		LAT2
NAA15			OCA2		LIMK1
POGZ			PAR1		MLXIPL
PTEN			PAR4		NCF1
RELN			PAR5		RFC2
SCN2A			PAR7		TBL2
SETD5			PWRN1		VPS37D
SHANK3			PWS		WBSCR11
SYNGAP1			SNORD115		WBSCR2
TBR1			SNORD116		WBSCR22
TRIP12			SNURF-SNRPN		WBSCR27
			UBE3A		

SI References

1. A. J. Holmes et al., Brain Genomics Superstruct Project initial data release with structural, functional, and behavioral measures. *Sci. Data.* **2**, 150031 (2015) https://doi.org/10.1038/sdata.2015.31

2. M. Jenkinson, P. Bannister, M. Brady, S. Smith, S, Improved optimization for the robust and accurate linear registration and motion correction of brain images. *Neuroimage.* **17**, 825–841 (2002) https://doi.org/10.1016/s1053-8119(02)91132-8